Analysis of Statistical Properties of Atmospheric Turbulence-Induced Image Dancing Based on Hilbert Transform and Dense Optical Flow

Jingyuan Liu, Bindang Xue, Linyan Cui
School of Astronautics, Beihang University, Beijing, China
Email: xuebd@buaa.edu.cn

***Abstract*—In this paper, the statistical properties of pixel displacements in turbulence degraded images are analyzed. Two main problems are addressed before that. One is the computation of pixel displacements. Dense optical flow is used since blur makes features like points and edges hard to track. The other one is selection of statistical samples. We use 2D-Hilbert transform to extract feature points, and only displacements at those points are considered. Statistical analysis includes distribution fitting, statistical parameters and normality test at different sample times and turbulence strengths. In the experiments, the method of computing distortions is first applied to simulated dataset to test its validity. Then this method of computing displacements and statistical analysis is applied to real-scene image sequences.**

Keywords—atmospheric turbulence; image dancing; optical flow; Hilbert transform; statistical analysis

I. INTRODUCTION

Optical turbulence is formed by the imhomogeneous distribution of temperature in atmospheric turbulence. It leads to a random fluctuation of refractive index and ultimately causes blur and distortions in turbulence degraded images. The core mechanism of this distortion is called wave-front angle-of-arrival(AOA) fluctuation, namely the random fluctuation of phase along the path from scene object to receiver aperture. The elimination of atmospheric turbulence-degraded effects is one of the main subjects in the study of optical imaging and image processing[1-5]. Meanwhile, these effects result from the interference of medium and light waves, thus can reflect some characteristics of the medium. AOA fluctuation is related to key parameters of optical turbulence, such as turbulence strength, turbulence inner and outer scale, and distance of optical path. Current studies utilize distortions in atmospheric turbulence-degraded images to retrieve AOA characteristics, and to estimate physical quantities such as turbulence inner scale[6], turbulence strength[7-9], crosswind strength and orientation[10], imaging distance[11], etc. Both the elimination of turbulence effects and the retrieval of turbulence parameters requires computing statistics such as variance, but there is no further study on statistical regularities. The statistical analysis of pixel displacements would benefit the study of statistical regularties of optical turbulence, and can work as a priori information in the elimination of turbulence effects.

In the work of image degrations simulation[12,13] and turbulence effects elimination[1-5], people typically make assumptions that pixel displacements in turbulence-degraded images are subjected to Gaussian random fields. In this paper, the statistical characteristics of pixel displacements are analyzed using image computing technology. The degration effects are a combination of image blur and distortion, and discontinuities at object boundaries are degrade into gray level transition intervals, thus common methods of computing motions by tracking feature points would fail to match the exact point of interest. Horn-Schunck(HS) optical flow solves a dense motion field in the image by minimizing global energy[14]. The optical flow vector at each pixel can be viewed as the pixel displacement. However, motions in less-textured regions are more likely to be affected by noise, so pixel displacements in rich-textured regions are preferred to be used for statistical analysis. Hilbert transform can convert discontinuities into local maximums, which has been widely used in edge detection[15]. In this paper, 2D-Hilbert transform and HS optical flow are combined to obtain relatively reliable pixel displacements. In this way, dense pixel displacements are firstly solved by optical flow, then those with less noise are screened using 2D-Hilbert transform.

In statistical analysis part, non-parametric kernel density estimation is utilized for fitting the possibility density function of pixel displacements[16]. It can estimate density function directly from data, without having to make an assumption of a particular distribution model. The displacements are assumed to be Gaussian in simulation, so we test the normality of the data[17] with respect to the Gaussian random field. Statistical parameters like variance, skewness and kurtosis are also computed at different sample times and turbulence strengths to study its statistical regularities. Finally, the same methods for computing pixel displacements and statistical analysis are performed on real-scene image sequences recorded in atmospheric turbulence conditions.

II. METHODS

A. Method description

The steps for image distortion statistical analysis are as follows. First, dense motion field in the image sequence is computed using HS optical flow[14]. Then, feature points are

extracted using 2D-Hilbert transform combined with a peak detector[15], and a mask indicating feature points is constructed. After that the motion field is selected in terms of the mask, and the optical flow vectors selected by the mask are considered as displacements of feature points. Finally, horizontal and vertical displacements of feature points are analyzed respectively, which includes computing variance, skewness and kurtosis, fitting possibility density curves, and normality tests. Figure 1 shows the flow chart for this process.

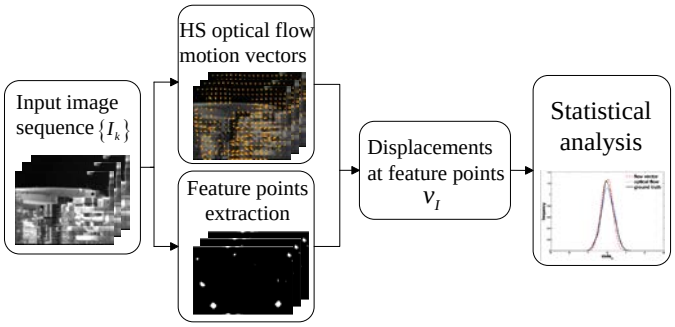

Fig. 1. Flow chart of the entire process

B. Pixel Displacements of Feature Points

In the first step, pixel displacements are obtained. Input image sequence is denoted as $\{I_k\}, k = 1,2,...,n$. Let the flow vector at point $\mathbf{x}=(x,y)$ be $\mathbf{v}=(v_x, v_y)$, which contains two components with respect to the horizontal and vertical direction. The object function of Horn-Schunck optical flow is based on intensity consistency model and the assumption that optical flow field varies smoothly:

$$\tilde{\mathbf{v}} = \arg\min \sum_{\mathbf{x}} \alpha_1 \left\| I_x v_x + I_y v_y + I_t \right\|^2 + \alpha_2 \left(\left\| \frac{\partial \mathbf{v}}{\partial x} \right\|^2 + \left\| \frac{\partial \mathbf{v}}{\partial y} \right\|^2 \right) \quad (1)$$

where I_x, I_y and I_t represent first derivative of intensity with respect to horizontal, vertical and time respectively. α_1 and α_2 are weights for data term and smooth term.

2D-Hilber transform is then applied to the image sequence. The detailed formula of Hilbert transform is given in [18], and its application in image processing is briefly listed here. Let the original image be a $N_1 \times N_2$ matrix $I[n_1, n_2]$, Hilbert transform is a signum funtion filtering process in frequency domain:

$$\hat{I}[k_1, k_2] = 2D - IDFT\left\{ H[n_1, n_2] \bullet DFT\left[I[n_1, n_2] \right] \right\} \quad (2)$$

where

$$H[n_1, n_2] = \begin{cases} -1, & n_1 = 1,2,...,N_1/2-1 \text{ and } n_2 = 1,2,...,N_2/2-1 \\ & \text{or } n_1 = N_1/2+1,...,N_1-1 \text{ and } n_2 = N_2/2+1,...,N_2-1 \\ 0, & n_1 = 0, N_1/2 \text{ or } n_2 = 0, N_2/2 \\ 1, & n_1 = 1,2,...,N_1/2-1 \text{ and } n_2 = N_2/2+1,...,N_2-1 \\ & \text{or } n_1 = N_1/2+1,...,N_1-1 \text{ and } n_2 = 1,2,...,N_2/2-1 \end{cases} \quad (3)$$

The absolute values of the result of Hilbert transform are taken and binarized with a threshold. The regions above the threshold are rich of textures. A peak detector is applied to the textured regions to extract feature points. In this paper, we use centroiding algorithm as a peak detector[15]. A feature point $(\bar{x}, \bar{y})$ is computed as:

$$\bar{x} = \frac{\sum_x \sum_y x \bullet I_{x,y}^2}{\sum_x \sum_y I_{x,y}^2}, \bar{y} = \frac{\sum_x \sum_y y \bullet I_{x,y}^2}{\sum_x \sum_y I_{x,y}^2} \quad (4)$$

As mentioned above, we regard the motion information provided by relatively textured regions as having higher confidence, thus only displacements at feature points are used for statistical analysis. Suppose the number of feature points is p. The coordinates of feature points are index for extracting corresponding horizontal and vertical displacements in the optical flow field. Selected vectors are denoted as v_I. The displacements vary with time, and form a bunch of displacements within the image sequence. Suppose a bunch of displacements varying with time at one feature point is regarded as a group of sample, then we obtained p groups of sample from one image sequence.

C. Methods for Statistical Analysis

The statistical methods involved in this paper include distribution fitting, computation of variance and higher-order moments, and normality test. For simulated datasets, the main purpose is to test that the statistical characteristics given by the method of this paper is consistent with ground truth, namely the results are consistent with the settings of Gaussian random fields in simulation. For real scene datasets, which are without grount truth, distribution fitting, normality test and computation of moments are applied.

Nonparametric kernel density estimation[16] is used to fit a distribution curve. The advantage of this approach is that it estimates density function using only sample data, without having to make an assumption of its distribution model and fit it with parameters.

Upon observing the distribution form from the graphs, normalities of the displacements is tested using Kolmogorov-Smirnov(KS) test[17], which measures the disparity between the sample cumulative distribution function and the theoretical cumulative distribution function. The null hypothesis is that the sample displacements comes from a distribution in the normal family, against the alternative that they do not come from such a distribution. Denote theoretical normal cumulative distribution function as $F_0(x)$, cumulative distribution function of displacements by $F_n(x)$, and disparity $D = \max\left|F_0(x) - F_n(x)\right|$. Null hypothesis is rejected when $D > D(n,\alpha)$, in which $D(n,\alpha)$ is the critical value for rejection at a significance level of α and sample size n. $D(n,\alpha)$ can be obtained by refering to the table in [17]. In this paper, a significance level $\alpha = 0.05$ is adopted.

The most commonly used statistical parameter in the literatures is variance, because it has a direct relationship with turbulence strength[19]. Besides variance, higher moments

parameters include skewness and kurtosis[20]. Equation(6) denotes skewness, which is defined as the ratio of third moment and cube of standard deviation to measure horizontal symmetry. If a distribution's scores are concentrated on the right side of the curve, it is left skewed and has a negative skewness. A normal distribution has a skewness value of zero. Kurtosis is defined as the ratio of fourth moment and square of variance as in (7), which identifies how concentrated the values are in the center of distribution. A normal distribution has a kurtosis value of three[20].

$$\text{variance} = \frac{1}{n-1}\sum_{k=1}^{n}\left(v_k - \bar{v}\right)^2 \tag{5}$$

$$skewness = \frac{1}{n}\sum_{k=1}^{n}\left(v_k - \bar{v}\right)^3 \Bigg/ \left(\sqrt{\frac{1}{n}\sum_{k=1}^{n}\left(v_k - \bar{v}\right)^2}\right)^3 \tag{6}$$

$$kurtosis = \frac{1}{n}\sum_{k=1}^{n}\left(v_k - \bar{v}\right)^4 \Bigg/ \left(\frac{1}{n}\sum_{k=1}^{n}\left(v_k - \bar{v}\right)^2\right)^2 \tag{7}$$

III. EXPERIMENTS

A. Simulated Data

In simulation experiments, turbulence degraded images are generated using an empirical model[12,13]. The approach of distortion simulation is by filtering a Gaussian random filed with a spatial correlation function. Upon Fourier inverse transform and normalization, simulated displacements are subjected to a Gaussian random field with mean value of zero and variance proportional to AOA variance. The original image is 256*256 sized gray level checkerboard. 5000 frames of simulated data are obtained under each set of parameters. Atmospheric turbulence parameters and imaging parameters used in simulation are listed in Table.1 and 2 respectively.

TABLE I. ATMOSPHERIC TURBULENCE PARAMETERS

Parameters	*Value*	*Unit*
Outer scale L_0	15	m
Inner scale l_0	5	mm
turbulence spectral index α	11/3	/

TABLE II. IMAGING PARAMETERS

Parameters	*Value*	*Unit*
Wave length λ	0.55	μm
Receiver aperture D	50	mm
Focal length f	55	mm
Angular resolution $\delta\theta$	0.2	urad

For weak turbulence(refractive index structure constant C_n^2 within range of 6.4×10^{-18} and $6\times10^{-17}m^{-2/3}$), 10 sample strengths are adopted and the corresponding imaging distance is $L=6000m$. For moderate-to-strong turbulence(refractive index structure constant C_n^2 within range of 6.4×10^{-15} and $2.5\times10^{-13}m^{-2/3}$), 10 sample strengths are adopted and the imaging distance is $L=1000m$. Only spherical waves are considered under such distances. Theoretical displacements computed during simulations are saved as ground truth for statistical analysis. Fig. 2 shows one simulated image and the feature point detection results.

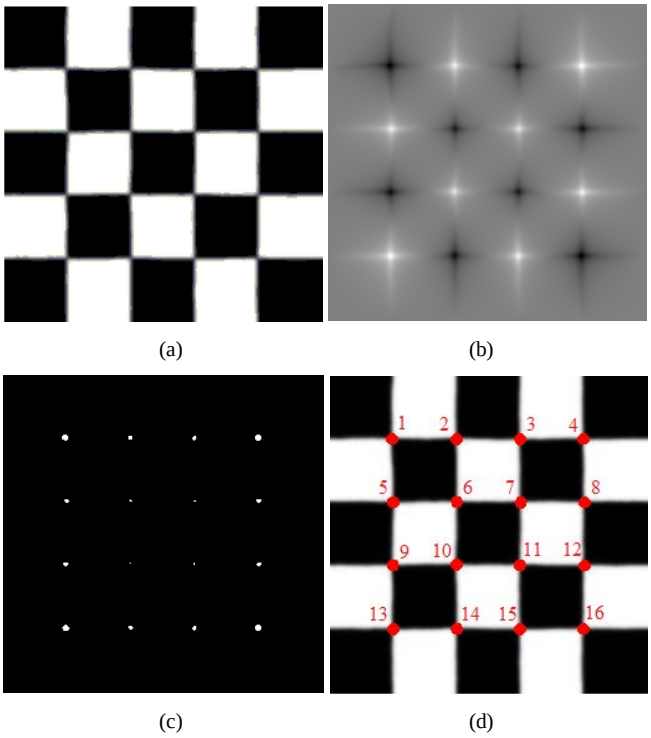

Fig. 2. Results under turbulence strength of $C_n^2 = 3.4\times10^{-14}m^{-2/3}$. (a)Simulated image; (b)result of Hilbert transform;(c)result of binarization;(d)result of feature point extraction.

16 feature points have been extracted, corresponding to 16 corners in the cherckerboard pattern. Results of fitting curves for displacements at each points show that curves for horizontal and vertical displacements are all of the bell curve as in normal distribution. Also, in moderate-to-strong turbulence distribution of displacements covers a wider range on x-axis than in weak turbulence. Take feature point number 6 as an example, the results for distribution fitting are shown in Fig.3.

In the following steps quantitative analysis are applied to both ground truth in simulations and displacements at feature points, including KS test and computation of statistical parameters. The results for feature point number 6 is shown in Table.3, in which "√" means to accept the null hypothesis, namely the displacements are subjected to a normal distribution, while "×" means to reject the null hypothesis. We find that for weak turbulence strengths greater than $C_n^2 = 4\times10^{-17}m^{-2/3}$ and all moderate-to-strong turbulence strengths, the statistical parameters are more likely to be close to ground truth, and are all able to accept null hypothesis in KS tests. This result primarily indicates that the method for computing displacements is more likely to get accurate results when

turbulence strength is greater than $C_n^2 = 4\times10^{-17} m^{-2/3}$. One possible reason is that when distortions are minor, displacements obtained from images are easily affected by computational accuracy limitations and noises. Under different turbulence strength conditions, variance of displacements increases proportionally with turbulence strength, while the values of skewness and kurtosis remain fluctuating around 0 and 3 respectively. There is no obvious tendency of the values of skewness and kurtosis varying with turbulence strength.

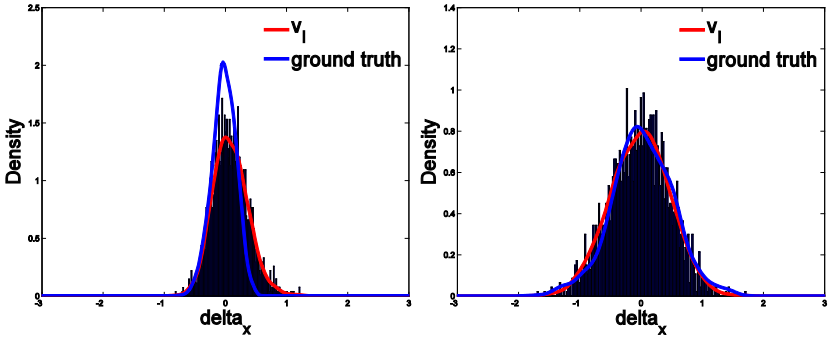

(a) (b)

Fig. 3. Horizontal displacements distribution curve at feature point number 6 under: (a)turbulence strength of $C_n^2 = 6\times10^{-17} m^{-2/3}$ (weak turbulence); (b) turbulence strength of $C_n^2 = 7.4\times10^{-14} m^{-2/3}$ (moderate-to-strong turbulence).

TABLE III. STATISTICAL PARAMETERS AT FEATURE POINT NUMBER 6 UNDER DIFFERENT TURBULENCE STRENGTH

strength		Weak turbulence						Moderate-to-strong turbulence					
		1×10^{-17}	2×10^{-17}	3×10^{-17}	4×10^{-17}	5×10^{-17}	6×10^{-17}	1.4×10^{-14}	3.4×10^{-14}	5.4×10^{-14}	7.4×10^{-14}	9.4×10^{-14}	1.4×10^{-13}
var	GT[a]	0.0079	0.0158	0.0235	0.0314	0.0388	0.0485	0.0532	0.1109	0.1789	0.2714	0.3031	0.4283
	CD[b]	0.0206	0.0406	0.0529	0.0635	0.0748	0.0930	0.0587	0.1131	0.1792	0.2435	0.2884	0.4191
skew	GT	0.0353	0.0108	0.0108	-0.0078	-0.0073	0.0086	0.0147	0.0389	0.0344	-0.0053	0.0064	-0.0149
	CD	0.1814	0.0962	0.1354	0.0815	0.1026	0.0963	-0.0110	-0.0243	0.0047	-0.0224	0.0012	-0.0174
kur	GT	2.9502	2.9277	2.9198	2.8927	2.8597	2.8956	2.8069	2.8573	2.9553	2.8055	3.2472	3.0686
	CD	3.5238	3.7718	3.3205	3.2473	3.1974	3.2937	2.8191	2.8235	2.8265	2.9047	2.9401	3.0644
KS	GT	√	√	√	√	√	√	√	√	√	√	√	√
	CD	×	×	√	√	√	√	√	√	√	√	√	√

[a] GT=Ground Truth

[b] CD=Computed Displacement

Finally we compute statistical parameters for pixel displacements of simulated data at different sample times. For a same set of simulation parameter, simulation is perform 10 times consequtively, and for each time 5000 frames of image data are generated. Since parameters setting in the simulation do not vary with times, experiment results show that statistical parameters of displacements also fluctuate around ground truth with times. Figure 4 shows how statistical parameters vary with times at feature point number 6 and 11 under turbulence strength $C_n^2 = 7.4\times10^{-14} m^{-2/3}$.

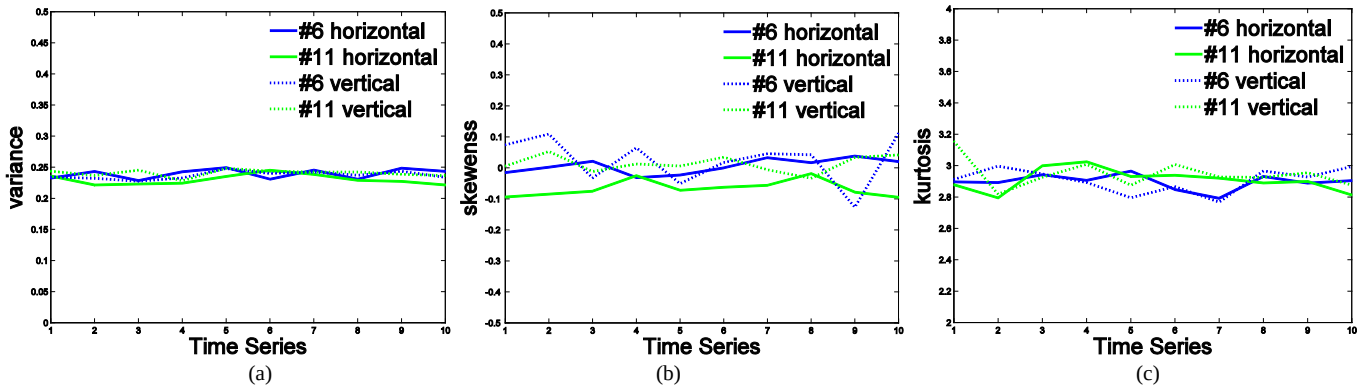

(a) (b) (c)

Fig. 4. Statistical parameters at feature point 6 and 11varying with times:(a)variance; (b)skewness;(c)kurtosis

B. *Real Scene Data*

In this section, the methods for computing displacements at feature points and statistical analysis are applied to real scene data. Image sequences are recorded using a BASLER acA1920-155um camera (150fps). Take car series as an example, a car is captured at different distances in a turbulence condition. Each sequence consists of 500 frames. The results of feature points extraction are shown in Fig.5.

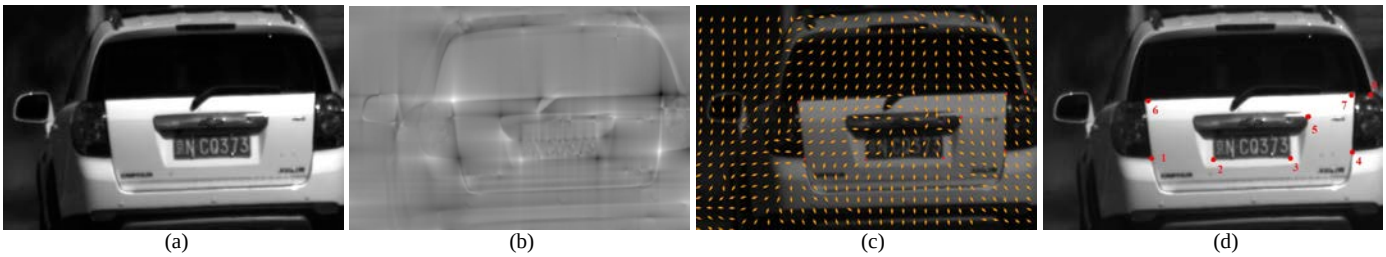

(a) (b) (c) (d)

Fig. 5. Feature Points extraction for car series: (a)recorded image; (b)result of Hilbert transform;(c)optical flow field;(d)8 feature points are extracted.

8 feature points are extracted from each frame. Optical flow field vectors at those points are collected as 8 groups of pixel displacements. Non-parametric kernel density estimation is applied to estimate distribution curve, and statistical parameters are computed at each feature point. The results for feature point 1~5 are shown in Fig.6 and Table 4. We observe that in real scene cases, distribution curves of displacements also appear to be bell curve as in normal distribution, while displacements of horizontal and vertical direction may show a significant discrepancy in statistical results. Since the 8 feature points are of the same imaging distance, this means real turbulence has different strengths along horizontal and vertical directions. Skewness and kurtosis fluctuate in a wider range compared with simulated cases. A too large kurtosis will lead to a rejection in KS test, such as point 3 in Table 4.

TABLE IV. STATISTICAL RESULTS FOR CAR SERIES

Mark		***1***	***2***	***3***	***4***	***5***
var	h[c]	2.7288	2.0162	2.0079	2.2782	2.9519
	v[d]	1.0750	1.1788	0.6137	1.1662	2.7820
skew	h	-0.0049	-0.1447	-0.6881	0.6943	-0.3284
	v	-0.1919	0.0064	0.5356	-0.2106	-0.2153
kur	h	4.0881	3.7236	4.2193	3.3828	3.6086
	v	3.4420	3.9356	4.5659	4.2699	3.9613
KS	h	×	√	√	√	√
	v	√	√	×	√	√

[c.] h=horizontal

[d.] v=vertical

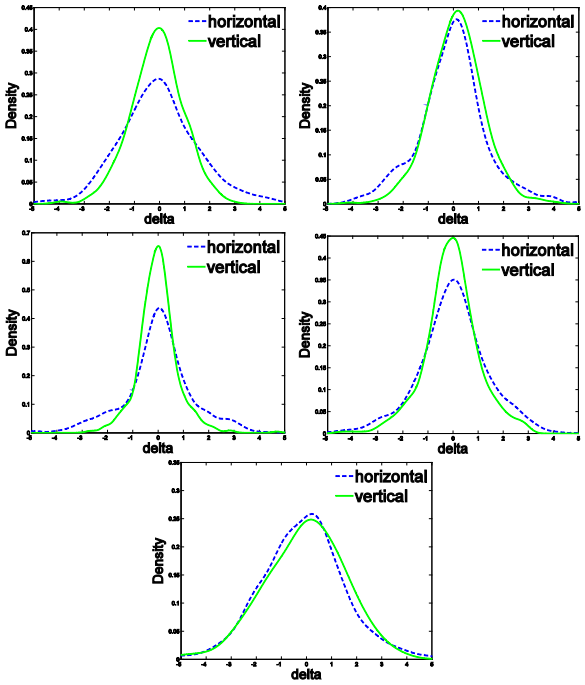

Fig. 6. Results of distribution curve fitting for feature points 1~5.

Fig.7 shows how statistical parameters at feature point 1 vary with time. For a fixed distance, variance of both horizontal and vertical displacements may vary dramatically with time, indicating dramatic fluctuations of turbulence strengths. Skewness and kurtosis still fluctuate around 0 and 3 respectively, but within a wider range compared with simulated cases. No obvious uniform tendency of statistical parameters varying with time is observed.

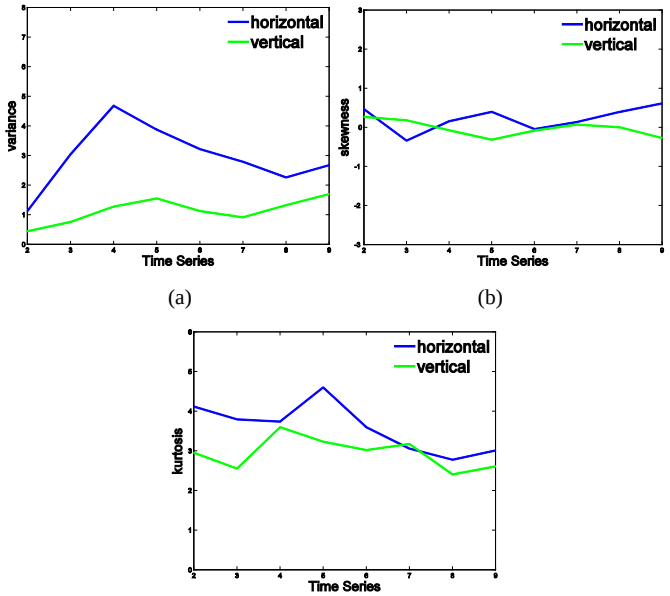

Fig. 7. Results of statistical parameters varying with time at feature point number 1:(a)variance;(b)skewness;(c)kurtosis.

IV. Conclusions

In this paper, statistical analysis of properties of atmospheric turbulence-induced image dancing is performed. Simulation experimental results show that for weak turbulence strengths greater than $C_n^2 = 4\times10^{-17} m^{-2/3}$ and all moderate-to-strong turbulence strengths, displacements are less likely to be affected by computational accuracy and noises, and the statistical parameters are close to ground truth. Distribution curves, KS test and higher moments parameters all indicate that displacements are subjected to normal distribution for turbulence strength which is greater than $C_n^2 = 4\times10^{-17} m^{-2/3}$. Real turbulence-induced image sequence experimental results show that variances of horizontal and vertical displacement show a dramatic discrepancy, and vary with time, while skewness and kurtosis remain fluctuating around 0 and 3 respectively. Most displacement samples in real scene can accept null hypothesis, indicating they are sujected to normal distribution.

References

[1] X. Zhu, P. Milanfar, “Removing Atmospheric Turbulence via Space-Invariant Deconvolution,” IEEE Trans. on PAMI, vol. 35, pp. 157–170, 2013.

[2] O. Oreifej, X.Li, et al, “Simultaneous Video Stabilization and Moving Object Detection in Turbulence,” IEEE Trans. on PAMI, vol. 35, pp. 450–462, 2013.

[3] Gibson, K.B, Nguyen, T.Q, “An Analysis and Method for Contrast Enhancement Turbulence Mitigation,” IEEE Trans. on Image processing, vol. 23, pp. 3179–3190, 2014.

[4] Mario Micheli, Yifei Lou,et al, “A Linear Systems Approach to Imaging Through Turbulence,” Journal of Mathematical Imaging and Vision, vol. 48, pp. 185–201, 2014.

[5] Ronen Gal, Nahum Kiryati,et al, “Progress in the restoration of image sequences degraded by atmospheric turbulence,” Pattern Recognition Letters, vol. 48, pp. 8–14, 2014.

[6] E. Masciadri,J. Vernin, “Optical technique for inner-scale measurement: possible astronomical applications,” Appl. Opt, vol. 36, pp. 1320–1327, 1997.

[7] Zamek, S., Yitzhaky, Y, “Turbulence strength estimation from an arbitrary set of atmospherically degraded images,” J. Opt. Soc. Am. A ,vol. 23, pp. 3106–3113, 2006.

[8] Gladysz S, “Estimation of turbulence strength directly from target images,” Opt. Soc. Am, vol. JW1A, pp. 4, 2013.

[9] M. Alterman, Y. Y. Schechner, et al, Passive tomography of turbulence strength, Springer International Publishing, 2014, pp. 47–60.

[10] O. Porat, J. Shapira, “Crosswind sensing from optical-turbulence-induced fluctuations measured by a video camera,” Appl. Opt, vol. 49, pp. 5236–5244, 2010.

[11] Y. Tian, S. G. Narasimhan, et al, “Depth from optical turbulence,” CVPR, pp. 246–253, 2012.

[12] Repasi E, Weiss R, “Analysis of image distortions by atmospheric turbulence and computer simulation of turbulence effects,” Proc. of SPIE 2008, Vol. 6941, 69410S-1–13.

[13] Repasi E, Weiss R, “Computer simulation of image degradations by atmospheric turbulence for horizontal views,” Proc. of SPIE 2011,Vol. 8014 80140U-1-9.

[14] Horn, B.K.P., and Schunck, B.G., “Determining Optical Flow,” Artificial Intelligence, pp. 185–203, 2004.

[15] Tavares P J D S, Má, Vaz R A, “Accurate subpixel corner detection on planar camera calibration targets,” Optical Engineering, vol. 46, pp. 107205-107205-8, 2007.

[16] Bowman A W, Azzalini A, Applied smoothing techniques for data analysis: the kernel approach with S-Plus illustrations, OUP Oxford, 1997, pp. 982.

[17] Lilliefors H W, “On the Kolmogorov-Smirnov test for normality with mean and variance unknown,” Journal of the American Statistical Association, vol. 62, pp. 399–402, 1967.

[18] Kohlmann K, “Corner detection in natural images based on the 2-D Hilbert transform,” Signal Processing, vol. 48, pp 225–234, 1996.

[19] Zamek S, Yitzhaky Y, “Turbulence strength estimation from an arbitrary set of atmospherically degraded images,” J. Opt. Soc. Am. A , vol. 23, pp. 3106–3113, 2007.

[20] Corder, G.W., and Foreman, D.I., Nonparametric Statistics for Non-Statisticians: A Step-by-Step Approach, Wiley, 2009, pp. 26–35.